


RESEARCH ARTICLE | JUNE 09 2023

Investigation of spin-orbit torque performance with W/Cu-multilayers as spin current source

B. Coester ; G. J. Lim ; F. N. Tan ; H. Y. Poh ; W. S. Lew  



Journal of Applied Physics 133, 223904 (2023)

<https://doi.org/10.1063/5.0139212>



CrossMark

AIP Advances

Why Publish With Us?

-  **25 DAYS**
average time to 1st decision
-  **740+ DOWNLOADS**
average per article
-  **INCLUSIVE**
scope

[Learn More](#)



Investigation of spin-orbit torque performance with W/Cu-multilayers as spin current source

Cite as: J. Appl. Phys. 133, 223904 (2023); doi: 10.1063/5.0139212

Submitted: 19 December 2022 · Accepted: 24 May 2023 ·

Published Online: 9 June 2023



B. Coester, G. J. Lim, F. N. Tan, H. Y. Poh, and W. S. Lew^{a)}

AFFILIATIONS

School of Physical & Mathematical Sciences, Nanyang Technological University, 21 Nanyang Link, Singapore 637371, Singapore

^{a)}Author to whom correspondence should be addressed: wensiang@ntu.edu.sg

ABSTRACT

We study the W/Cu multilayers as a spin current source and the coherent spin-orbit torques in a Fe layer using the spin-torque ferromagnetic resonance (STFMR) technique. With increasing numbers of layers, the line shape of the STFMR signals changes from predominantly antisymmetric to predominantly symmetric. When using $[W(0.5)/Cu(0.5)]_5$ as a spin current source, the symmetric amplitude increases by a factor of 5 compared to a single W layer. Simultaneously, the effective damping parameter also increases slightly due to enhanced spin pumping. Along with an increasing trend in the damping-like torque efficiency, this suggests that the extrinsic spin Hall effect is enhanced. Concurrently, the antisymmetric amplitude decreases significantly by a factor of 27, which indicates an increase in the field-like torque when multilayers are used as a spin current source.

Published under an exclusive license by AIP Publishing. <https://doi.org/10.1063/5.0139212>

I. INTRODUCTION

Current-induced spin-orbit torques (SOTs) have attracted substantial attention for magnetization control in ferromagnets (FMs) regarding energy-efficient memory applications.^{1–3} In a bilayer containing an FM and a nonmagnetic metal (NM) (FM/NM), the SOT can be generated via the Rashba-Edelstein effect (REE) or the spin Hall effect (SHE).^{4–6} The REE is the emergence of a spin accumulation at an interface due to structural inversion symmetry breaking and causes predominantly a field-like (FL) torque.^{3,7} On the other hand, the SHE is the generation of a transverse spin current, due to spin-dependent transverse velocities of the electrons, which exerts a predominantly damping-like (DL) torque onto magnetization upon absorption into the FM.^{3,7,8} The origin of the SHE can be caused by intrinsic^{9,10} or extrinsic effects, where the latter includes effects like skew scattering^{11–13} or side jump.^{8,14} In order to achieve a strong SOT, efforts have been made to improve charge-to-spin current conversion by using large spin-orbit coupled (SOC) materials such as W, Pt, or Ta^{4,10,15–18} or by enhancing the extrinsic SHE by doping or alloying, which provides more defects that lead to an increase in scattering events.^{19–24}

Recent studies have shown that inserting ultrathin layers at the FM/NM interface significantly influences the SOT performance.^{25–30} Additionally, it was shown by Zhu *et al.* that

inserting ultrathin Ti and Hf layers into the Pt layer effectively tuned the DL torque efficiency due to the enhancement of interfacial scattering.^{31,32} However, Hf has a short spin diffusion length of about 1 nm and, as a result, tends to attenuate spin currents.^{31,33} Hence, materials with a large spin diffusion length, like Cu, which has a spin diffusion length of several 100 nm,^{34,35} promise to overcome this issue. Furthermore, investigations utilizing Cu have shown to either enhance or diminish SOT, depending on the structure or fabrication technique. When sandwiched between a Pt and FM layer, Cu decreases SOT as it lowers the spin transparency of the interface,^{36,37} but when interfaced with a permalloy layer only, it can create a sizable FL torque.³⁸ Cu can also act as a potent doping material, enhancing the spin Hall conductivity in heavy metal (HM)-Cu alloys^{19,21,22} due to its high conductivity.

In this work, W/Cu multilayers were fabricated to investigate their spin-torque ferromagnetic resonance technique (STFMR) signals and SOT efficiencies as well as the effect on the damping in an adjacent Fe layer. While W acts as a spin current source, the insertion of Cu enhances interfacial scattering, without attenuating the spin current. The SOT efficiencies were determined for the NM multilayer by utilizing STFMR, as it allows extracting the effective damping parameter of the FM simultaneously.

II. METHODS

Stacks of Ti(2)/Fe(5)/NM(*x*)/Ti(5) (nominal thickness in nm) were fabricated by magnetron sputtering at room temperature onto thermally oxidized silicon wafers. The base pressure in the chamber was below 10^{-7} Torr and the pressure during the deposition was 2 mTorr for all layers. Devices of $5 \times 20 \mu\text{m}^2$ were patterned by a lithography lift-off process. The Ti layers were used as a seed layer and for oxidation prevention. For the NM multilayer, two sets were prepared. In set A, the total thickness of the NM multilayer remains constant at 5 nm and comprises *m*-repeats of [W/Cu]_{*m*}, where *m* ranges from 1 to 5. W and Cu are of equal nominal thicknesses. The total number of layers is *M* = 2*m*. In set B, W and Cu are both nominally 0.5 nm thick, with *n*-repeats of the [W(0.5)/Cu(0.5)]_{*n*} bilayer, where *n* ranges from 1 to 5. The corresponding total NM multilayer thicknesses range from 1 to 5 nm. The total number of layers is *N* = 2*n*. For the case of *M* = *N* = 10, sets A and B share the same NM multilayer configuration of [W(0.5)/Cu(0.5)]₅. Additionally, a sample with 5 nm W was fabricated and measured for comparison. The results were added to the results of sets A and B, indicated as *M* = *N* = 1.

The resistivity for the NM layers was measured using a four-point probe^{39–41} on separate thin films comprising only the NM layers and the seed and capping layer. The results are shown in Fig. 1(a) for set A and Fig. 1(b) for set B. The insets of the graphs show the conductivity of the NM multilayer. For set A, the resistivity increases with the number of layers due to the increased number of interfaces. Except for *M* = 2, where NM is W(2.5)/Cu(2.5), the resistivity drops slightly compared to the 5 nm W layer due to current shunting into the relatively thick Cu layer. For set B, the resistivity also increases with the number of layers due to interfacial scattering in the NM stack, although the overall thickness of the multilayer increases. This can be explained with a parallel resistor model of the multilayer, in which the interfaces must be included as resistors, as the thickness of the individual Cu and W layers is significantly smaller than the mean free path of the bulk materials.⁴² The resistor model is presented in the supplementary material. The resistivities for set B (*N* = 2, 4, 6, 8) are slightly higher than those of set A due to the thinner layers.

For the STFMR measurements, an alternating current (AC) with a power of *P* = 18 dBm at a radio frequency (RF) in the lower GHz range was sent into the device via the ground–source–ground RF probe. The AC was generated by a signal generator, connected to the RF port of a bias-T. The rectified DC voltage from the sample was measured by a lock-in amplifier, which was provided with a reference signal of 293 Hz from the low-frequency output of the signal generator. Figure 1(c) shows a schematic of the setup. The STFMR measurements were performed 20 times per sample and the results were averaged. All measurements were done at room temperature.

A typical STFMR signal measured at 15 GHz is shown in Fig. 1(d) and was fitted with⁴³

$$V_{\text{mix}} = V_0 + V_s F_S(H_{\text{ext}}) + V_a F_A(H_{\text{ext}}), \quad (1)$$

where $F_S(H_{\text{ext}}) = \Delta H^2 / [\Delta H^2 + (H_{\text{ext}} - H_{\text{res}})^2]$ and $F_A(H_{\text{ext}}) = \Delta H (H_{\text{ext}} - H_{\text{res}}) / [\Delta H^2 + (H_{\text{ext}} - H_{\text{res}})^2]$ are the symmetric and

antisymmetric Lorentzian functions, respectively. ΔH is the line-width (half width at half maximum—HWHM), H_{res} is the resonance field, H_{ext} is the applied static magnetic field, V_0 is a voltage offset, V_s and V_a are the amplitude of the symmetric and antisymmetric Lorentzian functions, respectively. V_s and V_a were then further used to calculate the FMR spin-torque efficiency as follows:^{43,44}

$$\xi_{\text{FMR}} = \frac{V_s e \mu_0 t_{\text{FM}} t_{\text{NM}} M_s}{V_a \hbar} \sqrt{1 + \frac{4\pi M_{\text{eff}}}{H_{\text{res}}}}, \quad (2)$$

where e is the electron charge, μ_0 is the vacuum permeability, t_{FM} is the thickness of the FM layer, t_{NM} is the thickness of the NM layer, M_s is the saturation magnetization, \hbar is the reduced Planck constant, and M_{eff} is the effective magnetization. M_{eff} can be determined from frequency-dependent measurements with the help of the Kittel equation for in-plane magnetized samples as $f = \gamma/2\pi \sqrt{H_{\text{res}} (H_{\text{res}} + 4\pi M_{\text{eff}})}$,⁴⁵ where γ is the gyromagnetic ratio.

III. RESULTS AND DISCUSSION

Figures 2(a) and 2(b) show the STFMR signals obtained for sets A and B at 15 GHz. Figure 2(a) also contains the results from the device with a 5 nm W layer (*M* = 1). In both sets, a change in line shape can be observed, going from dominantly antisymmetric for *M* = *N* = 1 or 2 to dominantly symmetric for *M* = *N* = 10. This is surprising as metallic bilayer systems with elemental or alloyed NM tend to exhibit a more dominantly antisymmetric shape,^{16,36,43,46–51} like the herein-used reference sample Fe(5)/W(5).

The change in line shape is also reflected in a rise in the FMR spin-torque efficiency, which is calculated with Eq. (2) and shown in Figs. 3(a) and 3(b) for sets A and B, respectively. The FMR spin-torque efficiency was initially proposed to give an estimate for the spin Hall angle (SHA),⁴³ which is the quantifying factor of charge-to-spin current conversion (and vice versa) for the SHE (ISHE). One notable benefit of the line shape analysis is that it is self-calibrated; i.e., all necessary parameters to calculate ξ_{FMR} (except for M_s and film thickness) can be obtained from the same measurement.^{43,52} Furthermore, it offers the possibility to gauge STFMR measurements when comparing FMR spin-torque efficiencies only. However, this method is not without limitations, and it is important to understand the main contributing components, which are the symmetric and antisymmetric Lorentzian amplitudes.

It was first assumed that the symmetric Lorentzian is generated by the DL effective field and the antisymmetric by the Oersted field.⁴³ Later on, it was shown that the symmetric Lorentzian can also be generated by spin pumping.⁴⁶ During the spin pumping process, the oscillating magnetization pumps a spin current into the adjacent NM, which is then transformed into a charge current via the ISHE.^{53–56} This leads to an overestimation of the SHA when calculating ξ_{FMR} . Similar to the symmetric Lorentzian, the antisymmetric Lorentzian also has another contributing component, namely, the FL effective field, typically assumed to be negligible.^{43,57} However, if the FL contribution is non-negligible, the FL

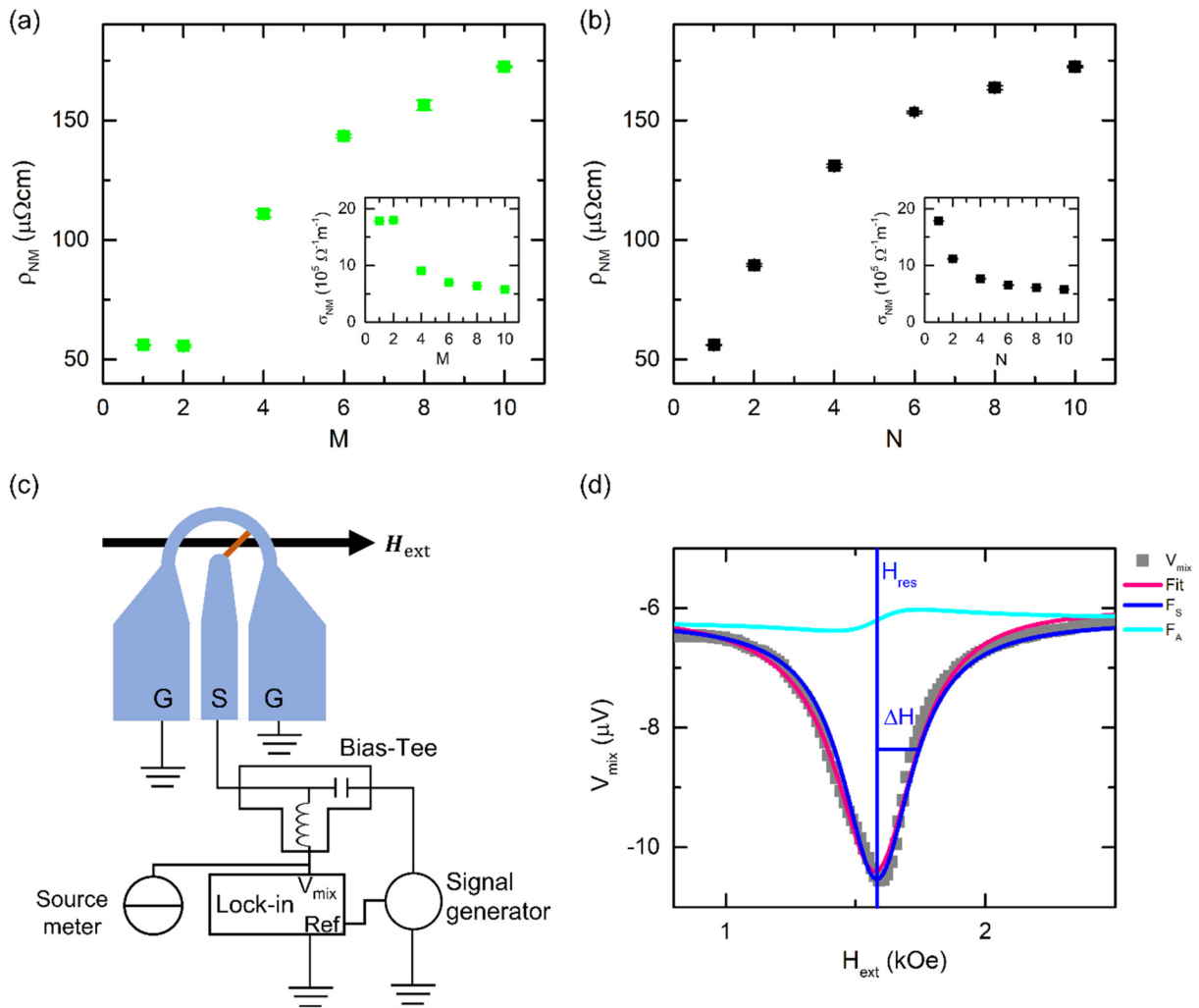


FIG. 1. Resistivity of the NM multilayers for (a) set A and (b) set B. The x axes of the graphs represent the number of layers. (c) Schematic of the pattern design and the measurement setup. (d) STFM signal for $[W(0.5)/Cu(0.5)]_5$ at 15 GHz (gray squares) with the corresponding fit (pink line). The dark and light blue lines are symmetric and antisymmetric Lorentzian functions, respectively.

effective field can subtract or add to the Oersted field contribution, depending on the relative sign between the two. As a result, this can lead to under- or overestimation of the SHA.³⁶

Here, the absolute value of the FMR spin-torque efficiency increases with the number of layers in the NM multilayer from $|\xi_{FMR}| = 0.07 \pm 0.006$ to $|\xi_{FMR}| = 5.54 \pm 3.12$, which is an increase by a factor of around 84. This is a much larger increase than in Cu and W alloyed systems, where the FMR spin-torque efficiency improves only up to a factor of 2.7.¹⁹ This could be an indication that the charge-to-spin current conversion or spin-to-charge current conversion, induced by interfacial scattering, is more efficient in NM multilayers than in alloyed or elemental W layers.^{19,31,32} The sign of ξ_{FMR} depends on the relative sign between the signs of the amplitudes. In set A, the sign of ξ_{FMR} changes at

$M = 4$ from positive to negative, and in set B, the sign is positive except for $N = 10$. Since the FMR spin-torque efficiency's main determining factor is the ratio of the symmetric and antisymmetric Lorentzian amplitude, it is worthwhile to examine them individually.

Figures 3(c) and 3(d) show the symmetric and antisymmetric amplitude for sets A and B. For both sets, V_s increases largely with increasing M and N , and V_a decreases with increasing M and N . The sign of V_s changes from positive to negative at $M = 4$ and $N = 2$. For set A, the sign of V_a remains positive for all samples, and in set B, it is negative for $N = 2$ to $N = 8$.

Since V_s can result either from the SHE-induced spin current traversing into the FM or from the spin current that is pumped into the NM, the increase in V_s must be the result of an enhanced

Downloaded from http://pubs.aip.org/jap/article-pdf/doi/10.1063/5.0139212/1799175/223904_1_5.0139212.pdf

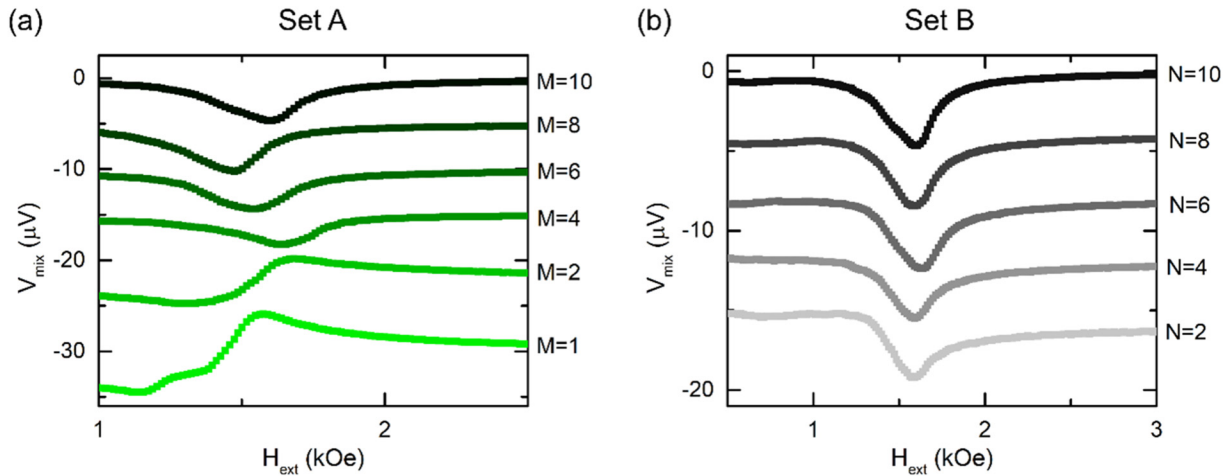


FIG. 2. STFM signal for 15 GHz for (a) set A, including the sample with 5 nm W layer ($M=1$) and (b) set B. The signals have been vertically offset for better comparison.

charge-to-spin current conversion or spin-to-charge current conversion. The cause for the enhancement is the increase in resistivity, i.e., scattering events, equivalent to the behavior in alloyed NM.^{20,58} Compared to the FMR spin-torque efficiency, the increase in V_s is only about a factor of 5. On the other hand, V_a decreases by a factor of 27 and is, thus, the more dominating factor for the change in the FMR spin-torque efficiency. The decrease in V_a occurs in both set A and set B. As V_a includes Oersted and FL torque contributions,⁴⁶ a plausible reason for the significant decrease could be the cancellation of the Oersted field torque by the FL torque.⁵⁹ However, it has to be noted that if that is the case, the FMR spin-torque efficiency loses its effectiveness in estimating the SHA.

To further distinguish the trends for spin pumping, DL, and FL torque efficiency, additional measurements were performed. To directly quantify the spin pumping contribution, 360° angular-dependent measurements are required,⁴⁶ which, however, are not feasible in our setup. Nonetheless, the effective damping, which can be extracted from frequency-dependent STFM measurements, depends significantly on spin pumping.⁶⁰ Therefore, the effective damping parameter is used as a guide for the spin pumping contribution in the NM multilayers.

The DL and FL torque efficiencies were determined from bias direct current (DC) STFM measurements. The DC was generated by a source meter and injected into the samples through the DC port of the bias-T.

The STFM signals measured at frequencies ranging from 12 to 28 GHz are shown in Fig. 4(a). From the frequency-dependent measurements, the effective damping parameter α_{eff} can be extracted from the linewidth, which was plotted against the resonance frequency and fitted with^{61,62}

$$\Delta H = \Delta H_0 + \alpha_{\text{eff}} \frac{2\pi}{\gamma} f, \quad (3)$$

where ΔH_0 is the inhomogeneous linewidth broadening due to magnetic inhomogeneities.⁶³

However, the data, as exemplified in Fig. 4(b), demonstrate non-linear behavior at the lower frequency range, which can stem from two-magnon scattering and slow relaxing impurity losses.^{61,64–66} Hence, linear fits are performed at higher frequencies where a linear behavior is observed. For consistency purposes, the fits start from 21 GHz onward for all samples. The results for the effective damping are shown in Figs. 4(c) and 4(d) for set A and set B, respectively. Set A shows a monotonic increase in the effective damping for $M=2$ onward. The trend for set B is similar, except for a saturation behavior at $N=8$ and $N=10$. The increase in the effective damping parameter can be explained by an increase in spin pumping contribution.^{34,54,55,60} With an increasing number of layers, the pumped spin current is converted more efficiently into a charge current via the ISHE.^{56,67–69} This is possible when the spin current that is pumped into the NM can travel through the Cu layers without significant attenuation due to the long spin diffusion length of Cu.³⁴ Consequently, W layers that are not adjacent to the FM can contribute to the ISHE.

The bias DC measurements, performed to separate DL and FL contributions, ideally show a linear behavior for the linewidth and the resonance field. From the slopes $\partial\Delta H/\partial J_{c, \text{NM}}$ and $\partial H_{\text{res}}/\partial J_{c, \text{NM}}$, the DL and FL torque efficiencies can be determined as follows:^{43,59}

$$\xi_{\text{DL}} = \frac{\gamma}{2\pi f} \frac{2e}{\hbar} \mu_0 M_s t_{\text{FM}} \left(\frac{H_{\text{res}} + 2\pi M_{\text{eff}}}{\sin\varphi} \right) \frac{\partial\Delta H}{\partial J_{c, \text{NM}}}, \quad (4)$$

$$\xi_{\text{FL}} = \frac{2e}{\hbar} \mu_0 M_s t_{\text{FM}}^{\text{eff}} \left\{ \left| \frac{\partial H_{\text{res}}}{\partial J_{c, \text{NM}}} \right| \frac{1}{\sin\varphi} - \frac{t_{\text{NM}}}{2} \right\}. \quad (5)$$

Figure 5(a) shows the I_{DC} -dependent measurements for the $[\text{W}(0.5)/\text{Cu}(0.5)]_5$ sample at 15 GHz. The I_{DC} -dependent linewidth

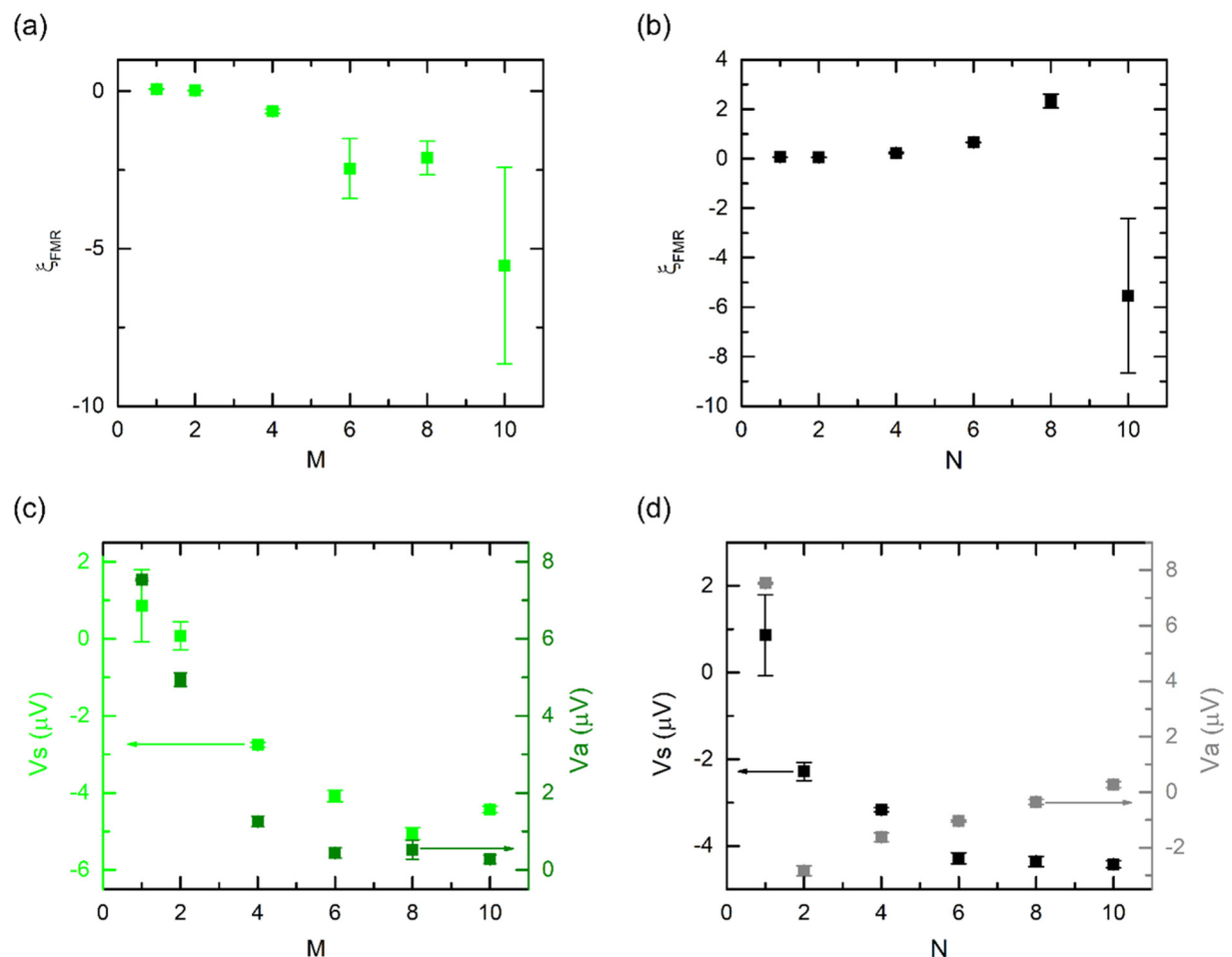


FIG. 3. FMR spin-torque efficiency for (a) set A and (b) set B. Symmetric and antisymmetric amplitude for (c) set A and (d) set B.

and resonance field are exemplified in Figs. 5(b) and 5(c) for the same sample, as well as the W(5) sample. The linewidth and the resonance field both show deviations from a linear behavior, which is due to Joule heating.⁵⁹ Thus, a quadratic term is added to the fitting function, and the parameters of the linear term are used to calculate the DL and FL torque efficiency with Eqs. (4) and (5), respectively. As the fitting window of DC-biased STFMR signals is very crucial, the fitting is repeated for several magnetic field ranges and the results are extrapolated to a zero fit window.⁷⁰ Details of the fitting and analysis as well as the fitting parameters are given in the supplementary material. The results for sets A and B for the DL and FL torque efficiencies are shown in Fig. 6.

The results for the DL torque efficiency in set A show an increasing trend from $M=1$ to $M=10$, with a maximum of $\xi_{\text{DL}} = 0.17 \pm 0.02$ for $M=8$. The increase in the DL torque efficiency from $M=4$ to $M=8$ can be explained by the increase in interfacial scattering.³¹ The increase in interfacial scattering is also reflected in the rise in the resistivity of the NM multilayers.

Importantly, the results suggest that the spin currents generated in the W layers that are not adjacent to the FM can travel through Cu, as discussed earlier for the damping enhancement, and can contribute to the DL torque efficiency.

By inserting Cu between the W layers, the sign changes from negative for $M=2$ to positive for $M=4$. In set B, the sign of the DL torque efficiency is positive for all samples, except for the reference sample $N=1$ with 5 nm W. The DL torque efficiencies for W and Cu have opposite signs when examined individually,^{7,34} caused by both intrinsic and extrinsic SHE.⁸ W has a negative sign, which agrees with the reference sample. W is also assumed to be the main source of the SHE-induced spin currents in the NM multilayers, and contributions from Cu are assumed to be negligible. Therefore, the change to a positive sign in set A from $M=4$ onwards, along with the positive sign in set B, could indicate that the extrinsic SHE dominates. This sign change in the SHA due to an extrinsic SHE was observed in diluted alloy systems.⁴⁹ Further investigations would help deepen the understanding of the extrinsic SHE in

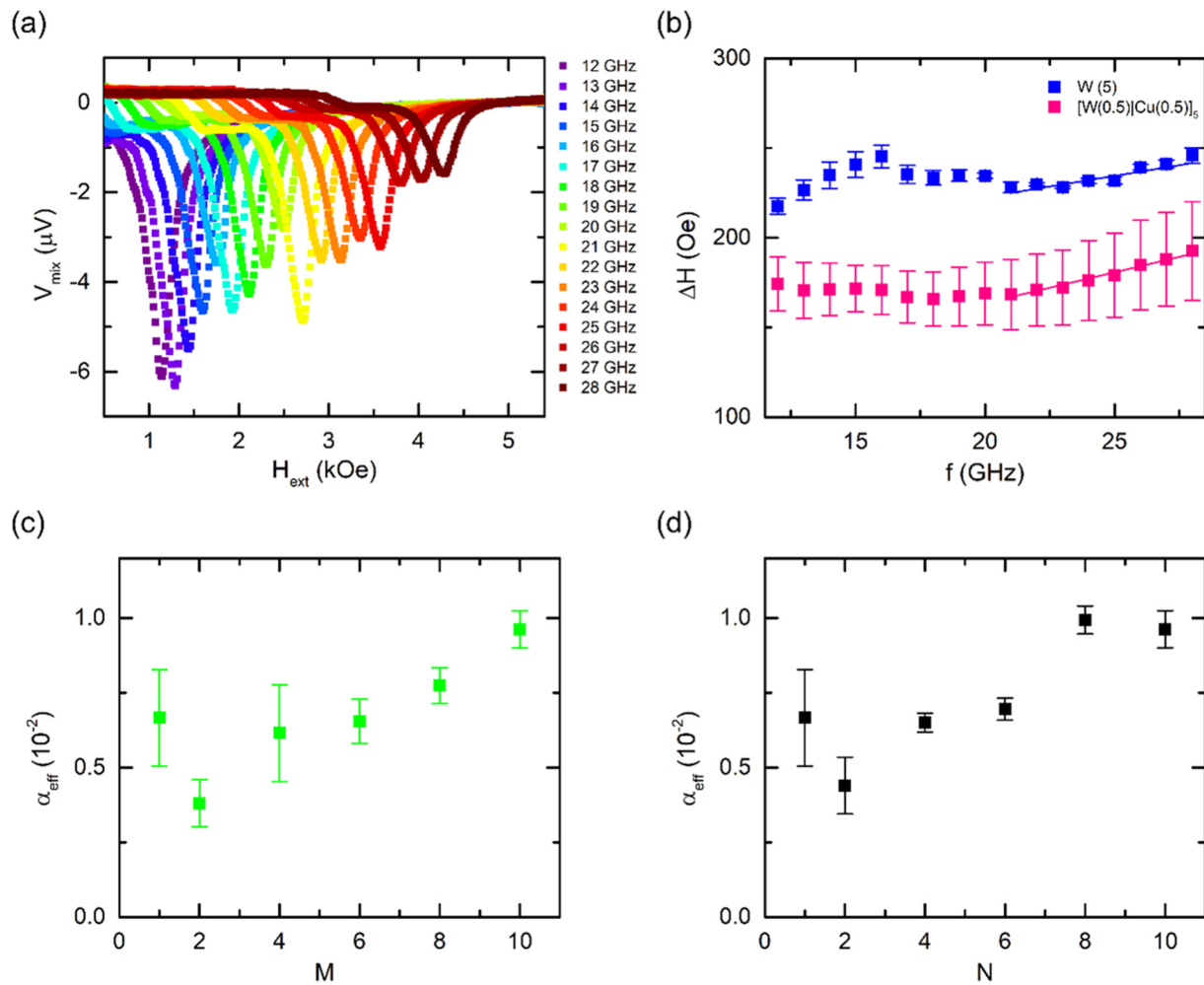


FIG. 4. (a) Frequency-dependent measurements of V_{mix} for $[\text{W}(0.5)/\text{Cu}(0.5)]_5$. (b) Frequency-dependent linewidth for samples with $[\text{W}(0.5)/\text{Cu}(0.5)]_5$ and $\text{W}(5)$ as NM. The linewidths show non-linear behavior at lower frequencies. The effective damping parameters were extracted at higher frequencies for (c) set A and (d) set B.

multilayer systems, but this is outside the scope of this paper. For $M=2$, the sign is negative as the 2.5 nm W layer adjacent to the Fe layer is comparably thick, allowing the effects from the W layer to dominate. This effect diminishes when more Cu layers are inserted and by decreasing the thickness of the layers.

In set B, the DL efficiency decreases from $N=2$ to $N=6$ before it increases at $N=8$ and then decreases again for $N=10$. At $N=8$, the DL torque efficiency reaches a maximum of $\xi_{\text{DL}} = 0.28 \pm 0.10$, while the smallest value is measured at $N=6$ with $\xi_{\text{DL}} = 0.08 \pm 0.06$. However, due to the larger error bars, it appears that the values scatter around a constant value. As the layer directly adjacent to the FM layer has the same thickness of 0.5 nm for all samples in set B, it would be conceivable to believe that only this layer contributes, resulting in a constant ξ_{DL} . If that was the case, in consequence, the DL torque efficiency for set A should be decreasing with increasing M , as the thickness of the adjacent layer

becomes thinner with increasing M .⁷¹ This is illustrated in Fig. S6 in the supplementary material, where the torque efficiency per unit electric field ξ_{DL}^E , which is the DL torque efficiency divided by the resistivity, i.e., $\xi_{\text{DL}}^E = \xi_{\text{DL}}/\rho_{\text{NM}}$, is plotted against the thickness of the W layer that is in direct contact with the FM layer. If only this layer contributes to ξ_{DL}^E , it will increase with increasing thickness,⁷¹ but the opposite is the case. This further confirms that consecutive layers contribute to the DL torque efficiency, which is in agreement with the results in Fig. 4. The increase in ξ_{DL} from $N=6$ to $N=8$ is assumed to be a result of the increase in interfacial scattering as discussed for set A.

The decrease in ξ_{DL} in set B from $N=2$ to $N=6$ is accompanied by an increase in the FL torque efficiency. The FL torque is a result of an exchange field generated by spin accumulation.³ The spin accumulation can be induced in the W layers by spin pumping because the thicknesses of the W layers are comparable to

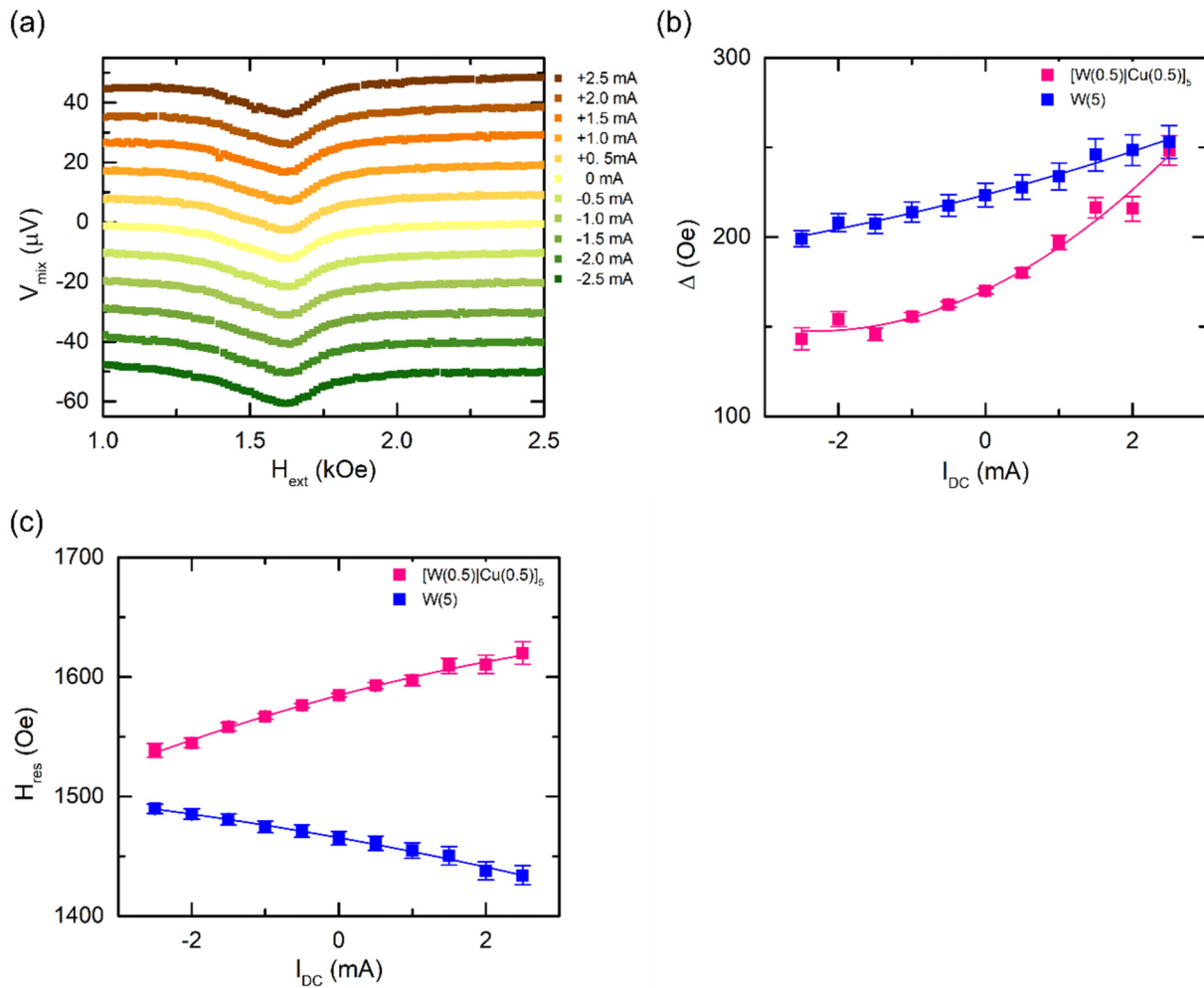


FIG. 5. Examples for I_{DC} measurements: (a) V_{mix} signals for the $[\text{W}(0.5)/\text{Cu}(0.5)]_5$ sample at 15 GHz. The curves are vertically offset for better comparison. (b) Linewidth and (c) resonance field vs bias DC at 15 GHz for samples with $[\text{W}(0.5)/\text{Cu}(0.5)]_5$ and W(5) as NM.

their spin diffusion length,^{8,35,72,73} which is about 2.1 nm.³⁴ Although it cannot be fully excluded that there is no spin accumulation in the Cu layers,⁷⁴ the long spin diffusion length of Cu^{34,35} suggests that the effect can be considered negligible in this work. Furthermore, it must be noted that in the bias DC STFMR method, only the net spin current that is absorbed by the FM contributes to the DL efficiency. Therefore, the complex interface effects and spin transparency of the FM/NM interface can play a crucial role,^{37,75–83} thereby potentially causing the decrease in ξ_{DL} .

The FL torque efficiency in both sets increases until $M = N = 6$ before it decreases again, appearing to saturate for set B. Since the FL torque is a result of an exchange field generated by spin accumulation,³ it is reasonable to assume that the increase in the FL torque efficiency until $M = 6$ and $N = 6$ is caused by spin accumulation. However, additional interfaces seem to not add further to the FL torque. The comparison of the trend of the

antisymmetric Lorentzian amplitude to the trend of the FL torque efficiency suggests that for larger numbers of M and N , Oersted and FL torques cancel each other out. However, when calculating the effective fields related to the efficiencies via $H_{\text{FL}} = (\hbar/2e)\xi_{\text{FL}}J_{\text{c,NM}}/(\mu_0 M_s t_{\text{FM}}^{\text{eff}})$ and $H_{\text{Oe,DC}} = J_{\text{c,NM}} t_{\text{NM}}/2$, which can be found in the supplementary material, H_{FL} is much larger than H_{Oe} , suggesting that still a net field should contribute to the antisymmetric Lorentzian and, therefore, it should not decrease as much. This could be an indication that the FL torque efficiency estimated by the bias DC STFMR technique is overestimated. In their work, Wang *et al.* reported an FL torque efficiency for a 5 nm thick as deposited W layer of $\xi_{\text{FL}} > 0.3$,⁸⁴ which agrees with the here extracted value of $\xi_{\text{FL}} = -0.30 \pm 0.18$. Other groups reported values that are around one order of magnitude smaller.^{46,59} A reason for the discrepancy could stem from different interfacial conditions. Wang *et al.* showed in their work that

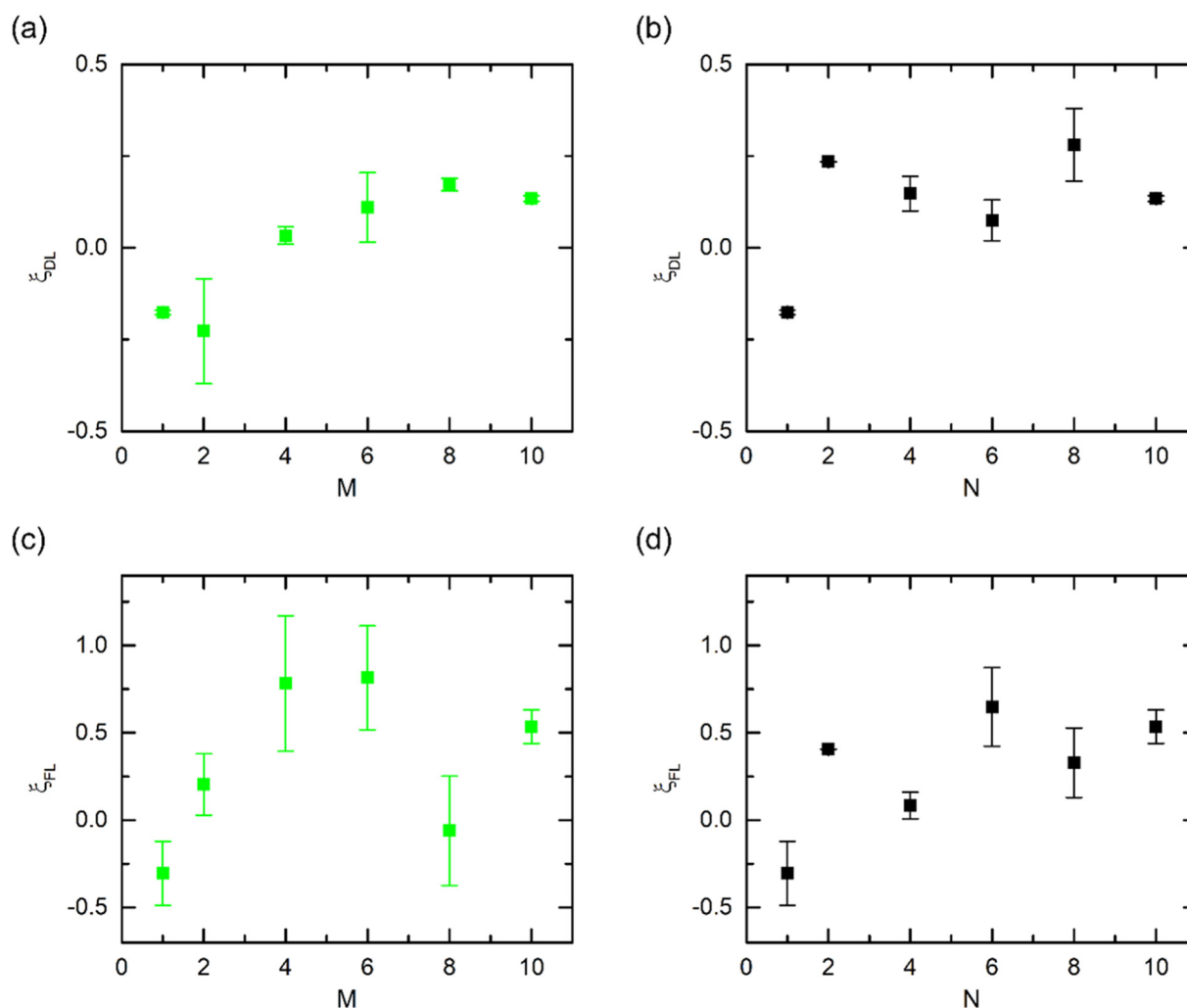


FIG. 6. (a) DL torque efficiency for set A and (b) set B and FL torque efficiency for (c) set A and (d) set B extracted from the bias current measurements.

the condition of the FM/W interface is very crucial for the strength of the FL torque. Upon increasing the spin transmission at the interface, the FL torque is reduced, as more spin current is absorbed into the FM and, thus, the spin accumulation is reduced.⁸⁴ We note that the herein-used FM layer is comparably thick to what is usually seen in reports for other materials.^{84–87} An additional reason could be the sensitivity in the analysis of the bias DC STFM. For our NM multilayer samples, the values of ξ_{FL} range from -0.06 ± 0.31 for $M = 8$ to 0.82 ± 0.29 for $M = 6$, which is within the range reported for metallic bilayer systems.⁷ A large FL torque could arise through additional effects like the REE,^{88–91} which is known to be experimentally hard to distinguish from the SHE^{7,72} or be an indication for an arising spin accumulation in the samples with NM multilayers due to spin pumping.^{8,71–73}

The here extracted DL torque efficiencies of the NM multilayer are similar to those reported for metallic bilayers⁷ and range from $\xi_{DL} = 0.03 \pm 0.02$ for $M = 4$ to $\xi_{DL} = 0.29 \pm 0.10$ for $N = 8$. However, to allow for a more conclusive interpretation of the values, it is advisable to have a closer look at ξ_{DL} of the reference sample $M = N = 1$ with a 5 nm W layer. Its DL torque efficiency of $\xi_{DL} = -0.18 \pm 0.01$ is within the range of reported values for tungsten;^{15,46,59,70} however, in most works, W is assumed to be in the β -phase or a mix of α - and β -phases, which should exhibit larger ξ_{DL} than the here assumed α -phase. For α -W, the DL torque efficiency is estimated to be around $\xi_{DL} = -0.03$ ⁹² or at least $\xi_{DL} < 0.07$.¹⁵ These values are closer to the result of the FMR spin-torque efficiency in Fig. 3 of $\xi_{FMR} = 0.07 \pm 0.01$. A difference between ξ_{DL} and ξ_{FMR} of one order of magnitude is not uncommon⁹³ but makes a proper quantification complex.

In order to check the trend of the SOT, additional harmonic hall measurements (HHMs) were performed, and the results were added in the supplementary material. The DL torque efficiencies show an increasing trend for both sets, which is agreeing well with the assumption that the added interfaces in the NM multilayer enhance the extrinsic SHE and that the spin currents are not attenuated by the Cu layers. Increases in the FL torque efficiency are still attributed to an increase in spin accumulation with more layers, although it is hard to discern a trend for set B, as the results are very noisy. In general, the FL torque efficiencies calculated from the HHM are much smaller, suggesting that its contribution is negligible, which then would mean that the FMR spin-torque efficiency from Fig. 3 is a valid estimation of the spin Hall angle if the spin pumping contribution is small. As ξ_{FMR} is still larger than the DL torque efficiency estimated from the HHM, and the damping parameter is enhanced in Fig. 4, the discrepancy between the two is partly attributed to spin pumping. However, the observed significant decrease in the antisymmetric Lorentzian amplitude for higher layer numbers cannot be fully explained with a reduction in the Oersted field, as H_{Oe} reduces only by a factor of 2 for set A from $M = 1$ to $M = 10$, while V_a reduces by a factor of 27, and in set B, the Oersted field even increases from $N = 2$ to $N = 10$ by a factor of 2, where V_a decreases by a factor of 10. Another possibility for the reduction in the antisymmetric amplitude is related to changes in the resistance of the device. The amplitudes are dependent on the RF current⁴³ I_{rf} and related to the resistance of the device in a relation as follows: $V_{\text{sa}} \propto I_{\text{rf}} = \sqrt{P/R}$. Given a larger/smaller device resistance, the amplitudes should decrease/increase with $1/\sqrt{R}$, assuming that all other factors and the SOT are constant across all samples. However, the changes in $1/\sqrt{R}$ are relatively modest for set A, by only a factor of about 1.3. For set B, the resistance decreases from $N = 2$ to $N = 10$ due to the increase in the thickness; therefore, V_a should increase; however, it still decreases by a factor of 10.

Therefore, these observations suggest that the change in the antisymmetric amplitude cannot be fully explained by the changes in resistance or Oersted field and that the FL torque likely contributes significantly to the signal. For set A, where both V_a and the Oersted field are decreasing, it can be assumed that the FL torque increases until it almost compensates for the Oersted field torque. Similarly, for set B, where H_{Oe} even increases, the FL torque must increase as well, as V_a is decreasing and changing in sign. As discussed above, the increase in the FL torque could originate in the enhancement in the SHE but also in the REE. As the REE is an interfacial effect, the addition of layers and interfaces in the NM might amplify this effect.

As the symmetric component is also proportional to $1/\sqrt{R}$, it is necessary to evaluate how much the change in resistance contributes to the signal. In set A, where the resistance increases, the symmetric amplitude also increases, therefore deviating from the expected $1/\sqrt{R}$, which suggests that the effect of the resistance on V_s is negligible. In contrast for set B, where V_s increases by a factor of 1.9 from $N = 2$ to $N = 10$, which is comparable to the expected increase of a factor of 1.1 due to the $1/\sqrt{R}$ dependence. Furthermore, the changes in resistance cannot account for the changes in sign observed in the amplitudes.

Regarding the discrepancy in efficiency values determined from the bias DC STFM measurements and HHM, a possible explanation could be the low current density changes in the bias DC STFM measurements. The current densities in the NM multilayer vary in the high 10^{10} - low 10^{11} A/m² range, resulting in rather large slopes $\partial\Delta H/\partial J_{\text{c,NM}}$ and $\partial H_{\text{res}}/\partial J_{\text{c,NM}}$. In the literature, the DC-induced current densities are usually about 10^{12} A/m² or larger.⁵⁹ However, for more than $I_{\text{DC}} = 2.5$ mA, the signal-to-noise ratio decreased significantly. Additionally, the fitting is very sensitive to the applied fitting range.

IV. CONCLUSION

In conclusion, we have investigated NM multilayers comprising alternating W and Cu layers regarding their potential as the spin current source. STFM signals show a significant shift in line shape from predominantly antisymmetric to predominantly symmetric with increasing numbers of W/Cu layers. The symmetric Lorentzian amplitude increases by a factor of 5 from a single W layer to a sample with $[\text{W}(0.5)/\text{Cu}(0.5)]_5$ as NM with the same total thickness. While an increase in the effective damping parameter shows a contribution from the spin pumping effect due to an enhancement in ISHE, investigations of the DL efficiency also indicate the enhancement of the extrinsic SHE. At the same time, a notable reduction in the antisymmetric Lorentzian amplitude by a factor of 27 is found in the same set of samples. This reduction cannot solely be explained by a decrease in the Oersted field or a change in the resistance in the samples, as their anticipated effects are only around a factor of 2 and 1.1, respectively. Similarly, in the second set of samples with varying thicknesses, changes in sign occur in V_a , which cannot stem from the changes in resistance or H_{Oe} either. Therefore, the results suggest that the FL torque changes with the introduction of multilayers into the NM.

SUPPLEMENTARY MATERIAL

See the supplementary material for the resistor model of the NM multilayer, the absolute values for the FMR spin-torque efficiency and amplitudes, the detailed description of the bias current measurement analysis, the efficiency per unit electric field, Oersted and FL effective field calculation, and results of harmonic Hall measurements.

ACKNOWLEDGMENTS

This work was supported by the RIE2020 ASTAR AME IAF-ICP grant via Grant No. I1801E0030.

AUTHOR DECLARATIONS

Conflict of Interest

The authors have no conflicts to disclose.

Author Contributions

B. Coester: Conceptualization (equal); Formal analysis (equal); Funding acquisition (equal); Validation (equal); Writing – original draft (equal). **G. J. Lim:** Writing – review & editing (equal). **F. N. Tan:** Writing – review & editing (equal). **H. Y. Poh:** Investigation

(supporting); Writing – review & editing (equal). **W. S. Lew:** Funding acquisition (equal); Supervision (equal).

DATA AVAILABILITY

The data that support the findings of this study are available from the corresponding author upon reasonable request.

REFERENCES

- ¹C. O. Avci, A. Quindeau, C.-F. Pai, M. Mann, L. Caretta, A. S. Tang, M. C. Onbasli, C. A. Ross, and G. S. D. Beach, *Nat. Mater.* **16**(3), 309–314 (2017).
- ²J. Ryu, S. Lee, K.-J. Lee, and B.-G. Park, *Adv. Mater.* **32**(35), 1907148 (2020).
- ³E. Y. Vedmedenko, R. K. Kawakami, D. D. Sheka, P. Gambardella, A. Kirilyuk, A. Hirohata, C. Binek, O. Chubykalo-Fesenko, S. Sanvito, B. J. Kirby, J. Grollier, K. Everschor-Sitte, T. Kampfrath, C. Y. You, and A. Berger, *J. Phys. D: Appl. Phys.* **53**(45), 453001 (2020).
- ⁴L. Liu, O. J. Lee, T. J. Gudmundsen, D. C. Ralph, and R. A. Buhrman, *Phys. Rev. Lett.* **109**(9), 096602 (2012).
- ⁵G. Yu, P. Upadhyaya, Y. Fan, J. G. Alzate, W. Jiang, K. L. Wong, S. Takei, S. A. Bender, L.-T. Chang, Y. Jiang, M. Lang, J. Tang, Y. Wang, Y. Tserkovnyak, P. K. Amiri, and K. L. Wang, *Nat. Nanotechnol.* **9**(7), 548–554 (2014).
- ⁶F. Luo, Q. Y. Wong, S. Li, F. Tan, G. J. Lim, X. Wang, and W. S. Lew, *Sci. Rep.* **9**(1), 10776 (2019).
- ⁷A. Manchon, J. Železný, I. M. Miron, T. Jungwirth, J. Sinova, A. Thiaville, K. Garello, and P. Gambardella, *Rev. Mod. Phys.* **91**(3), 035004 (2019).
- ⁸J. Sinova, S. O. Valenzuela, J. Wunderlich, C. H. Back, and T. Jungwirth, *Rev. Mod. Phys.* **87**(4), 1213–1260 (2015).
- ⁹D. Xiao, M.-C. Chang, and Q. Niu, *Rev. Mod. Phys.* **82**(3), 1959–2007 (2010).
- ¹⁰M. Morota, Y. Niimi, K. Ohnishi, D. H. Wei, T. Tanaka, H. Kontani, T. Kimura, and Y. Otani, *Phys. Rev. B* **83**(17), 174405 (2011).
- ¹¹J. Smit, *Physica* **24**(1), 39–51 (1958).
- ¹²M. Gradhand, D. V. Fedorov, P. Zahn, and I. Mertig, *Phys. Rev. Lett.* **104**(18), 186403 (2010).
- ¹³Y. K. Kato, R. C. Myers, A. C. Gossard, and D. D. Awschalom, *Science* **306**(5703), 1910–1913 (2004).
- ¹⁴L. Berger, *Phys. Rev. B* **2**(11), 4559–4566 (1970).
- ¹⁵C.-F. Pai, L. Liu, Y. Li, H. W. Tseng, D. C. Ralph, and R. A. Buhrman, *Appl. Phys. Lett.* **101**(12), 122404 (2012).
- ¹⁶L. Liu, C.-F. Pai, Y. Li, H. W. Tseng, D. C. Ralph, and R. A. Buhrman, *Science* **336**(6081), 555, (2012).
- ¹⁷M. I. Dyakonov and V. I. Perel, *Phys. Lett. A* **35**(6), 459–460 (1971).
- ¹⁸*Spin Physics in Semiconductors*, 2nd ed. (Springer, Cham, 2017).
- ¹⁹B. Coester, G. D. H. Wong, Z. Xu, J. Tang, W. L. Gan, and W. S. Lew, *J. Magn. Mater.* **523**, 167545 (2021).
- ²⁰R. Ramaswamy, Y. Wang, M. Elyasi, M. Motapothula, T. Venkatesan, X. Qiu, and H. Yang, *Phys. Rev. Appl.* **8**(2), 024034 (2017).
- ²¹G. D. H. Wong, W. C. Law, F. N. Tan, W. L. Gan, C. C. I. Ang, Z. Xu, C. S. Seet, and W. S. Lew, *Sci. Rep.* **10**(1), 9631 (2020).
- ²²Z. Xu, G. D. Hwee Wong, J. Tang, E. Liu, W. Gan, F. Xu, and W. S. Lew, *ACS Appl. Mater. Interfaces* **12**, 32898 (2020).
- ²³P. Laczkowski, J.-C. Rojas-Sánchez, W. Saverio-Torres, H. Jaffrès, N. Reyren, C. Deranlot, L. Notin, C. Beigné, A. Marty, J.-P. Attané, L. Vila, J.-M. George, and A. Fert, *Appl. Phys. Lett.* **104**(14), 142403 (2014).
- ²⁴K. Tian and A. Tiwari, *Sci. Rep.* **9**(1), 3133 (2019).
- ²⁵M.-H. Nguyen, C.-F. Pai, K. X. Nguyen, D. A. Muller, D. C. Ralph, and R. A. Buhrman, *Appl. Phys. Lett.* **106**(22), 222402 (2015).
- ²⁶H.-Y. Lee, S. Kim, J.-Y. Park, Y.-W. Oh, S.-Y. Park, W. Ham, Y. Kotani, T. Nakamura, M. Suzuki, T. Ono, K.-J. Lee, and B.-G. Park, *APL Mater.* **7**(3), 031110 (2019).
- ²⁷M. Mann and G. S. D. Beach, *APL Mater.* **5**(10), 106104 (2017).
- ²⁸D. Li, B. Cui, T. Wang, J. Yun, X. Guo, K. Wu, Y. Zuo, J. Wang, D. Yang, and L. Xi, *Appl. Phys. Lett.* **110**(13), 132407 (2017).
- ²⁹H. Almasi, M. Xu, Y. Xu, T. Newhouse-Illige, and W. G. Wang, *Appl. Phys. Lett.* **109**(3), 032401 (2016).
- ³⁰S. K. Li, X. T. Zhao, W. Liu, Y. H. Song, L. Liu, X. G. Zhao, and Z. D. Zhang, *Appl. Phys. Lett.* **114**(8), 082402 (2019).
- ³¹L. Zhu, L. Zhu, S. Shi, M. Sui, D. C. Ralph, and R. A. Buhrman, *Phys. Rev. Appl.* **11**(6), 061004 (2019).
- ³²L. Zhu and R. A. Buhrman, *Phys. Rev. Appl.* **12**(5), 051002 (2019).
- ³³Y. Ou, C.-F. Pai, S. Shi, D. C. Ralph, and R. A. Buhrman, *Phys. Rev. B* **94**(14), 140414 (2016).
- ³⁴H. L. Wang, C. H. Du, Y. Pu, R. Adur, P. C. Hammel, and F. Y. Yang, *Phys. Rev. Lett.* **112**(19), 197201 (2014).
- ³⁵J. Bass and W. P. Pratt, *J. Phys.: Condens. Matter* **19**(18), 183201 (2007).
- ³⁶T. Nan, S. Emori, C. T. Boone, X. Wang, T. M. Oxholm, J. G. Jones, B. M. Howe, G. J. Brown, and N. X. Sun, *Phys. Rev. B* **91**(21), 214416 (2015).
- ³⁷W. Zhang, W. Han, X. Jiang, S.-H. Yang, and S. S. P. Parkin, *Nat. Phys.* **11**(6), 496–502 (2015).
- ³⁸R. W. Greening, D. A. Smith, Y. Lim, Z. Jiang, J. Barber, S. Dail, J. J. Heremans, and S. Emori, *Appl. Phys. Lett.* **116**(5), 052402 (2020).
- ³⁹F. M. Smits, *Bell Syst. Tech. J.* **37**(3), 711–718 (1958).
- ⁴⁰L. Valdes, *Proc. IRE* **42**(2), 420–427 (1954).
- ⁴¹H. Topsoe, *Bulletin* **472**(13), 63 (1968).
- ⁴²H. C. Chen, H. W. Chen, S. P. Jeng, C. M. M. Wu, and J. Y. C. Sun, presented at the *2006 International Symposium on VLSI Technology, Systems, and Applications, Hsinchu, Taiwan, 24–26 April 2006* (IEEE, 2006).
- ⁴³L. Liu, T. Moriyama, D. C. Ralph, and R. A. Buhrman, *Phys. Rev. Lett.* **106**(3), 036601 (2011).
- ⁴⁴C.-F. Pai, Y. Ou, L. H. Vilela-Leão, D. C. Ralph, and R. A. Buhrman, *Phys. Rev. B* **92**(6), 064426 (2015).
- ⁴⁵C. Kittel, *Phys. Rev.* **73**(2), 155–161 (1948).
- ⁴⁶A. Okada, Y. Takeuchi, K. Furuya, C. Zhang, H. Sato, S. Fukami, and H. Ohno, *Phys. Rev. Appl.* **12**(1), 014040 (2019).
- ⁴⁷Y. Wang, P. Deorani, X. Qiu, J. H. Kwon, and H. Yang, *Appl. Phys. Lett.* **105**(15), 152412 (2014).
- ⁴⁸L. Huang, S. He, Q. J. Yap, and S. T. Lim, *Appl. Phys. Lett.* **113**(2), 022402 (2018).
- ⁴⁹A. Musha, Y. Kanno, and K. Ando, *Phys. Rev. Mater.* **3**(5), 054411 (2019).
- ⁵⁰J. Zhou, X. Wang, Y. Liu, J. Yu, H. Fu, L. Liu, S. Chen, J. Deng, W. Lin, X. Shu, H. Y. Yoong, T. Hong, M. Matsuda, P. Yang, S. Adams, B. Yan, X. Han, and J. Chen, *Sci. Adv.* **5**(5), eaau6696 (2019).
- ⁵¹C. Hong, L. Jin, H. Zhang, M. Li, Y. Rao, B. Ma, J. Li, Z. Zhong, and Q. Yang, *Adv. Electron. Mater.* **4**(8), 1700632 (2018).
- ⁵²M.-H. Nguyen and C.-F. Pai, *APL Mater.* **9**(3), 030902 (2021).
- ⁵³Y. Tserkovnyak, A. Brataas, G. E. W. Bauer, and B. I. Halperin, *Rev. Mod. Phys.* **77**(4), 1375–1421 (2005).
- ⁵⁴Y. Tserkovnyak, A. Brataas, and G. E. W. Bauer, *Phys. Rev. B* **66**(22), 224403 (2002).
- ⁵⁵Y. Tserkovnyak, A. Brataas, and G. E. W. Bauer, *Phys. Rev. Lett.* **88**(11), 117601 (2002).
- ⁵⁶F. D. Czeschka, L. Dreher, M. S. Brandt, M. Weiler, M. Althammer, I. M. Imort, G. Reiss, A. Thomas, W. Schoch, W. Limmer, H. Huebl, R. Gross, and S. T. B. Goennenwein, *Phys. Rev. Lett.* **107**(4), 046601 (2011).
- ⁵⁷G. D. Hwee Wong, Z. Xu, W. Gan, C. C. I. Ang, W. C. Law, J. Tang, W. Zhang, P. K. J. Wong, X. Yu, F. Xu, A. T. S. Wee, C. S. Seet, and W. S. Lew, *ACS Nano* **15**(5), 8319–8327 (2021).
- ⁵⁸M. Isasa, E. Villamor, L. E. Hueso, M. Gradhand, and F. Casanova, *Phys. Rev. B* **91**(2), 024402 (2015).
- ⁵⁹C. Kim, D. Kim, B. S. Chun, K.-W. Moon, and C. Hwang, *Phys. Rev. Appl.* **9**(5), 054035 (2018).
- ⁶⁰L. Flacke, L. Liensberger, M. Althammer, H. Huebl, S. Geprägs, K. Schultheiss, A. Buzdakov, T. Hula, H. Schultheiss, E. R. J. Edwards, H. T. Nembach, J. M. Shaw, R. Gross, and M. Weiler, *Appl. Phys. Lett.* **115**(12), 122402 (2019).

- ⁶¹H. T. Nembach, T. J. Silva, J. M. Shaw, M. L. Schneider, M. J. Carey, S. Maat, and J. R. Childress, *Phys. Rev. B* **84**(5), 054424 (2011).
- ⁶²J. M. Shaw, H. T. Nembach, and T. J. Silva, *Phys. Rev. B* **85**(5), 054412 (2012).
- ⁶³M. Weiler, G. Woltersdorf, M. Althammer, H. Huebl, and S. T. Goennenwein, *Solid State Physics* (Elsevier, 2013), Vol. 64, pp. 123–156.
- ⁶⁴G. Woltersdorf and B. Heinrich, *Phys. Rev. B* **69**(18), 184417 (2004).
- ⁶⁵M. Körner, K. Lenz, R. A. Gallardo, M. Fritzsche, A. Mücklich, S. Facsko, J. Lindner, P. Landeros, and J. Fassbender, *Phys. Rev. B* **88**(5), 054405 (2013).
- ⁶⁶I. Barsukov, F. M. Römer, R. Meckenstock, K. Lenz, J. Lindner, S. Hemken to Krax, A. Banholzer, M. Körner, J. Grebing, J. Fassbender, and M. Farle, *Phys. Rev. B* **84**(14), 140410 (2011).
- ⁶⁷E. Saitoh, M. Ueda, H. Miyajima, and G. Tatara, *Appl. Phys. Lett.* **88**(18), 182509 (2006).
- ⁶⁸H. Y. Inoue, K. Harii, K. Ando, K. Sasage, and E. Saitoh, *J. Appl. Phys.* **102**(8), 083915 (2007).
- ⁶⁹K. Ando, Y. Kajiwara, S. Takahashi, S. Maekawa, K. Takemoto, M. Takatsu, and E. Saitoh, *Phys. Rev. B* **78**(1), 014413 (2008).
- ⁷⁰S. Karimeddy and D. C. Ralph, *Phys. Rev. Appl.* **15**(6), 064017 (2021).
- ⁷¹M.-H. Nguyen, D. C. Ralph, and R. A. Buhrman, *Phys. Rev. Lett.* **116**(12), 126601 (2016).
- ⁷²M. Althammer, *J. Phys. D: Appl. Phys.* **51**(31), 313001 (2018).
- ⁷³H. Jiao and G. E. W. Bauer, *Phys. Rev. Lett.* **110**(21), 217602 (2013).
- ⁷⁴J. Ding, W. Zhang, M. B. Jungfleisch, J. E. Pearson, H. Ohldag, V. Novosad, and A. Hoffmann, *Phys. Rev. Res.* **2**(1), 013262 (2020).
- ⁷⁵J. C. Rojas-Sánchez, N. Reyren, P. Laczkowski, W. Savero, J. P. Attané, C. Deranlot, M. Jamet, J. M. George, L. Vila, and H. Jaffrès, *Phys. Rev. Lett.* **112**(10), 106602 (2014).
- ⁷⁶S. A. Bender and Y. Tserkovnyak, *Phys. Rev. B* **91**(14), 140402 (2015).
- ⁷⁷L. Zhu, D. C. Ralph, and R. A. Buhrman, *Phys. Rev. Lett.* **123**(5), 057203 (2019).
- ⁷⁸M. Weiler, M. Althammer, M. Schreier, J. Lotze, M. Pernpeintner, S. Meyer, H. Huebl, R. Gross, A. Kamra, J. Xiao, Y.-T. Chen, H. Jiao, G. E. W. Bauer, and S. T. B. Goennenwein, *Phys. Rev. Lett.* **111**(17), 176601 (2013).
- ⁷⁹K. Gupta, R. J. H. Wesselink, R. Liu, Z. Yuan, and P. J. Kelly, *Phys. Rev. Lett.* **124**(8), 087702 (2020).
- ⁸⁰X. Waintal, E. B. Myers, P. W. Brouwer, and D. C. Ralph, *Phys. Rev. B* **62**(18), 12317–12327 (2000).
- ⁸¹Y. Liu, Z. Yuan, R. J. H. Wesselink, A. A. Starikov, and P. J. Kelly, *Phys. Rev. Lett.* **113**(20), 207202 (2014).
- ⁸²L. Zhu, D. C. Ralph, and R. A. Buhrman, *Phys. Rev. B* **99**(18), 180404 (2019).
- ⁸³L. Wang, R. J. H. Wesselink, Y. Liu, Z. Yuan, K. Xia, and P. J. Kelly, *Phys. Rev. Lett.* **116**(19), 196602 (2016).
- ⁸⁴Z. Wang, H. Cheng, K. Shi, Y. Liu, J. Qiao, D. Zhu, W. Cai, X. Zhang, S. Eimer, D. Zhu, J. Zhang, A. Fert, and W. Zhao, *Nanoscale* **12**(28), 15246–15251 (2020).
- ⁸⁵J. Kim, J. Sinha, M. Hayashi, M. Yamanouchi, S. Fukami, T. Suzuki, S. Mitani, and H. Ohno, *Nat. Mater.* **12**(3), 240–245 (2013).
- ⁸⁶I. Mihai Miron, G. Gaudin, S. Auffret, B. Rodmacq, A. Schuhl, S. Pizzini, J. Vogel, and P. Gambardella, *Nat. Mater.* **9**(3), 230–234 (2010).
- ⁸⁷K. Garello, I. M. Miron, C. O. Avci, F. Freimuth, Y. Mokrousov, S. Blügel, S. Auffret, O. Boulle, G. Gaudin, and P. Gambardella, *Nat. Nanotechnol.* **8**(8), 587–593 (2013).
- ⁸⁸V. M. Edelstein, *Solid State Commun.* **73**(3), 233–235 (1990).
- ⁸⁹V. V. Bel'kov and S. D. Ganichev, *Semicond. Sci. Technol.* **23**(11), 114003 (2008).
- ⁹⁰I. M. Miron, K. Garello, G. Gaudin, P.-J. Zermatten, M. V. Costache, S. Auffret, S. Bandiera, B. Rodmacq, A. Schuhl, and P. Gambardella, *Nature* **476**(7359), 189–193 (2011).
- ⁹¹H. Kurebayashi, J. Sinova, D. Fang, A. C. Irvine, T. D. Skinner, J. Wunderlich, V. Novák, R. P. Campion, B. L. Gallagher, E. K. Vehstedt, L. P. Zárbo, K. Výborný, A. J. Ferguson, and T. Jungwirth, *Nat. Nanotechnol.* **9**(3), 211–217 (2014).
- ⁹²K. Fritz, S. Wimmer, H. Ebert, and M. Meinert, *Phys. Rev. B* **98**(9), 094433 (2018).
- ⁹³K.-U. Demasius, T. Phung, W. Zhang, B. P. Hughes, S.-H. Yang, A. Kellock, W. Han, A. Pushp, and S. S. P. Parkin, *Nat. Commun.* **7**(1), 10644 (2016).